Supporting Information for

Highly Conductive and Solution-Processable Micro-Hydrogels of Nanoparticle/Graphene Platelets Produced by Reversible Self-Assembly and Aqueous Exfoliation

Nhien H. Le,[a] Humaira Seema,[a] K. Christian Kemp,[a] Nisar Ahmed,[a] Jitendra N. Tiwari,*[a] Sungjin Park,[b] and Kwang S. Kim*[a]

[a] Center for Superfunctional Materials, Department of Chemistry, Pohang University of Science and Technology, Hyojadong, Namgu, Pohang 790-784, Korea.

[b] Department of Chemistry, Inha University, 100 Inha-ro, Nam-gu, Incheon 402-751, Korea.

*E-mail: kim@postech.ac.kr, jnt_tiw123@yahoo.co.in

1. Electrostatic interaction

The influence of pH condition (ionization degree) on the colloidal suspension was investigated. After sonochemical treatment for 2 hours, the mixtures of SnO_2/chemically converted graphene (CCG) platelets were adjusted to different pH using hydrochloric acid for acidic solutions and aqueous ammonium hydroxide for alkaline solutions. Then the suspensions were kept in a static condition to observe their colloidal stability over time. After one day, the suspensions with pH 2, 7 and 14 sediment while the suspension at pH 10 was still stable without considerable sedimentation. This can be attributed to the effect of electrostatic repulsion among negatively charged SnO_2/CCG platelets in the suspension at pH 10. This result agrees with studies of colloidal reduced graphene oxide in aqueous suspensions.[1]

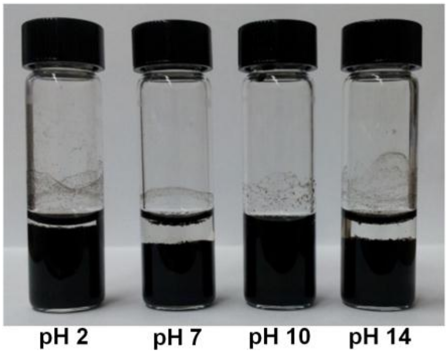

Fig. S1 Suspensions of sonochemically converted SnO_2/CCG in different pH (2, 7, 10 and 14) after one day in a static condition.

2. Structural characterization

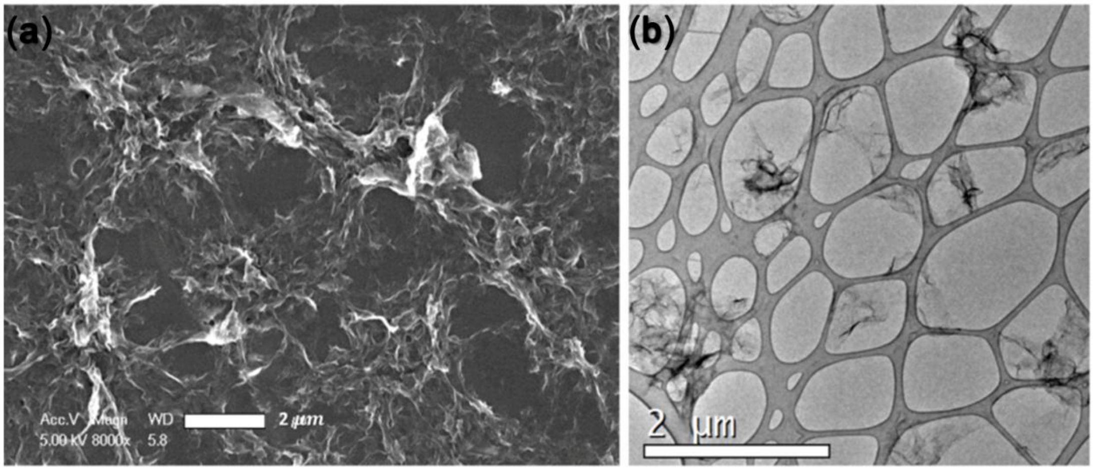

Fig. S2 Distribution of micro-assemblies of SnO_2/CCG platelets. (a) SEM image of micronanogels. (b) TEM image of the micronanogels.

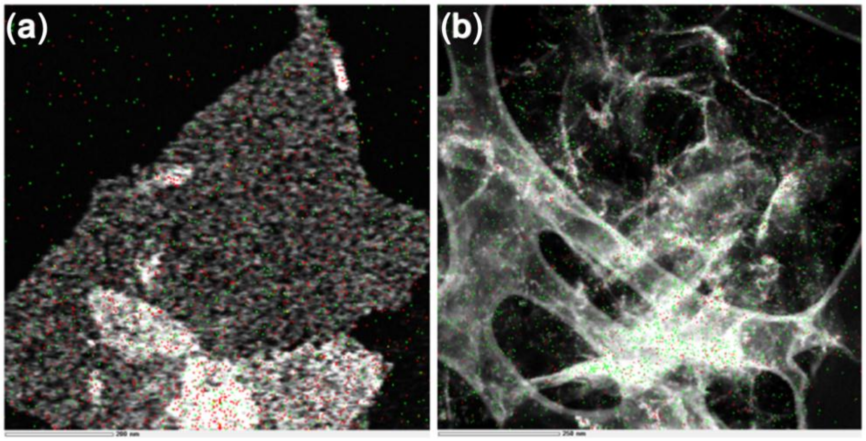

Fig. S3 Elemental mapping (red dot: Sn, green dot: O) of the sonochemically converted SnO_2/CCG nanoplatelet (a) and the micronanogel (b).

3. Morphological formation

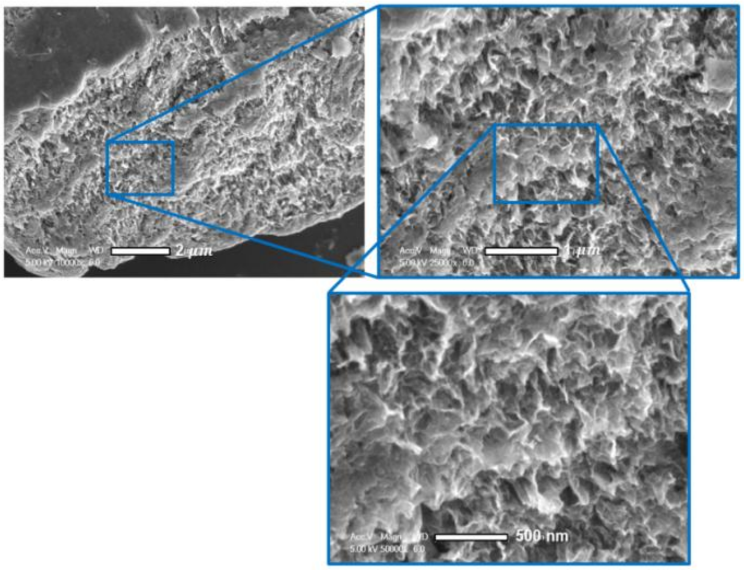

Fig. S4 SEM images of calcinated SnO_2/CCG nanocomposite (drypowder).

For comparison, SnO_2/CCG composites were synthesized without the use of sodium ascorbate, and CCG hydrogels were prepared without the use of stannous ions or SnO_2 nanoparticles. The same amounts of chemicals (G-O, $SnCl_2$ and sodium ascorbate) were used, but either $SnCl_2$ or sodium ascorbate was not added to the reactions. Both reactions were heated for 3 hours to induce the agglomeration of the nanocomposites in the aqueous solutions, while the principal reaction with both $SnCl_2$ and sodium ascorbate produced cylindrical bulk material after 90 minutes.

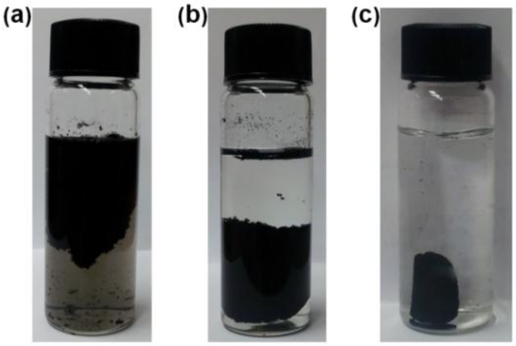

Fig. S5 Digital photographs of CCG hydrogel without adding $SnCl_2$ after static heating for 3 hours (a), SnO_2/CCG nanocomposite without adding sodium ascorbate after static heating for 3 hours (b) and SnO_2/CCG hydrogel using both $SnCl_2$ and sodium ascorbate (macronanogels) after static heating for 90 minutes (c).

SEM was used to visualize the microscale morphologies of the CCG-based materials. When stannous ions or ascorbic agents are absent, the driving forces of aggolomeration are reduced. After 90-minute heating, CCG hydrogels (without nanoparticles) and SnO_2/CCG (without sodium ascorbate) have low porosity (Figures S4a and S4b). However, after heating for 3 hours, SEM images in Figures S4c and S4d show pore formation in both the CCG hydrogel and the SnO_2/CCG. This suggests that the higher degree of self-assembly could be responsible for the porous 3D structure of macronanogel (Figure S4e).

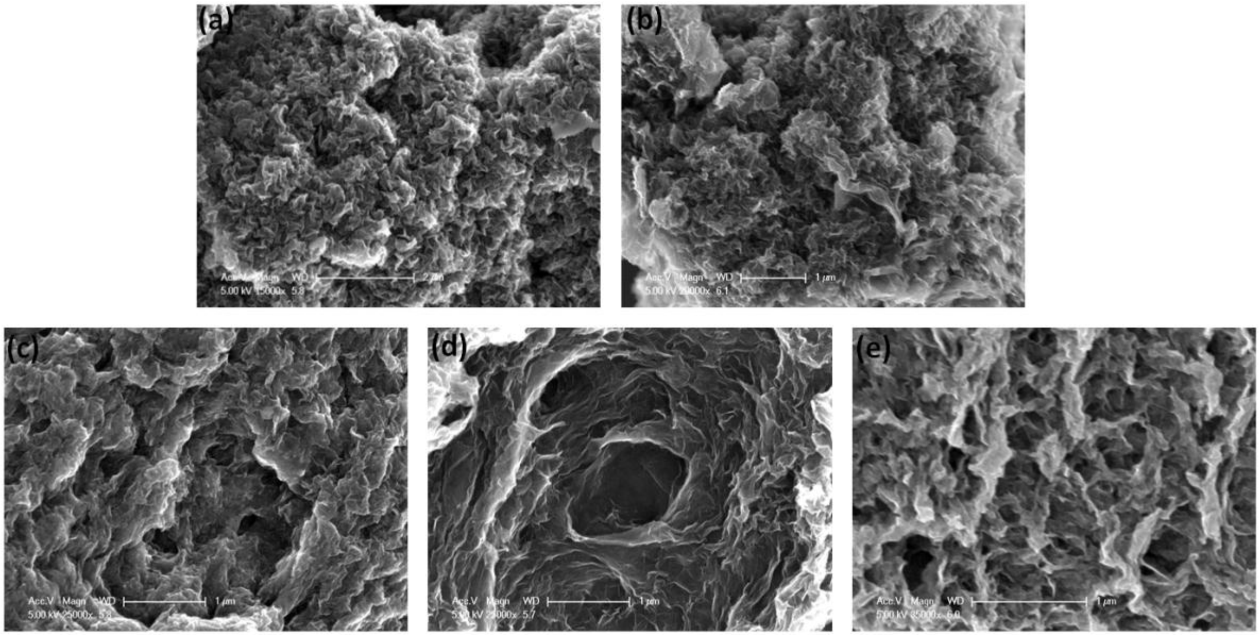

Fig. S6 SEM images of CCG hydrogels without using $SnCl_2$ after static heating in 90 minutes (a) and 3 hours (c). SEM images of SnO_2/CCG without using sodium ascorbate after static heating in 90 minutes (b) and 3 hours (d). SEM image of macronanogels (e).

4. Ultrasonic re-dispersibility

Portions of the CCG hydrogel and SnO_2/CCG hybrids were transferred to 20 ml water, followed by sonication. Then the suspensions were diluted to visualize colloids in aqueous medium. For the CCG hydrogel, even after ultrasonic re-dispersion for 12 hours, small aggregated particles in the suspension were visible (Figure S2a), revealing the irreversible hydrophobic π-π stacking of CCG platelets. For SnO_2/CCG nanocomposites, the agglomerated structure showed good re-dispersibility in water through the formation of a homogenous suspensions after 1 hour of sonication (Figures S2b,c). The nanoparticle decoration plays an important role as hydrated nanospacers that effectively hinder the π-π stacking of CCG platelets. Macronanogels with higher degree of self-assembly as well as water encapsulation could be ultrasonically exfoliated into micronanogels (Figure S2c).

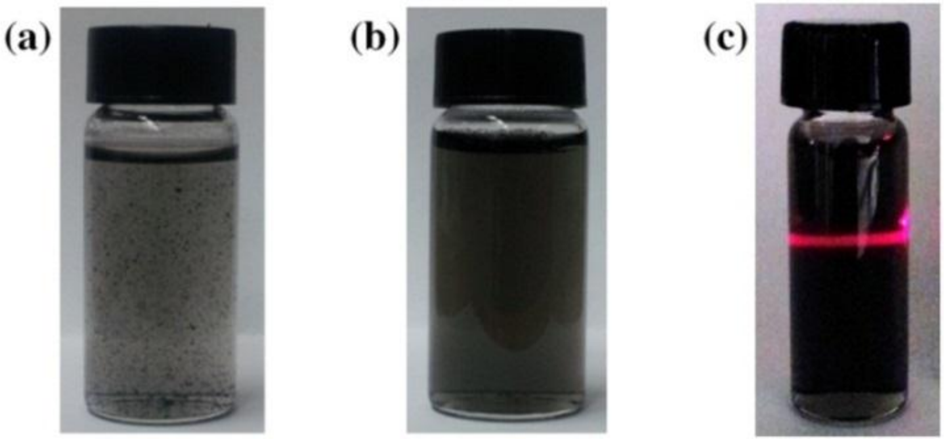

Fig. S7 (a) CCG hydrogel with the absence of SnO_2 after ultrasonic treatment for 12 hours. (b) SnO_2/CCG composite without using SA after ultrasonic treatment for 1 hour. (c) Suspension of micronanogel after sonicating macronanogels for 1 hour with Tyndall scattering effect.

5. Specific-surface-area measurements

The SnO_2/CCG composite prepared by conventional sol-gel method and SnO_2/CCG composites derived from the macronanogels and the micronanogels were investigated. The materials were heat-treated at 200 ^oC to dehydrate completely before specific surface area (SSA) measurement. BET surface areas were calculated from N_2 adsorption–desorption isotherms measured at 77 K. The results show that the SnO_2/CCG composite prepared by conventional method has a SSA of 177 m^2 g^{-1} and the SnO_2/CCG composite derived from the macronanogels has a SSA of 331 m^2 g^{-1}. In addition, with additional ultrasonic treatment to exfoliate the macronanogels into the micronanogels, the dry nanocomposite derived from the micronanogels shows a SSA of 364 m^2 g^{-1}.

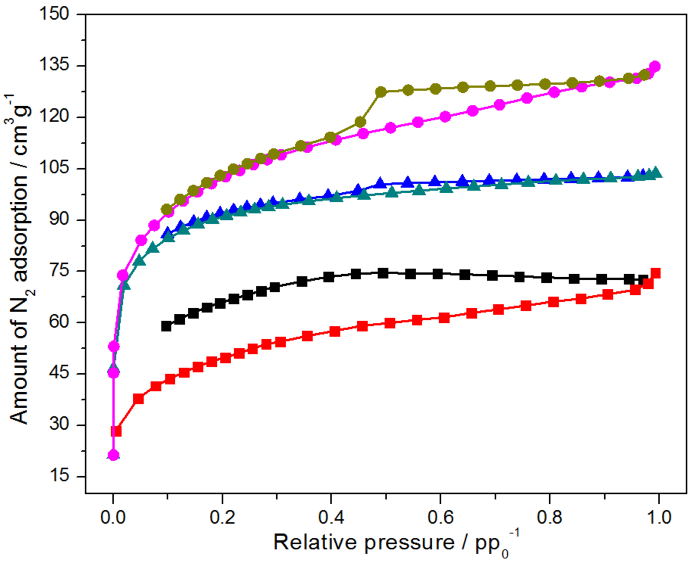

Fig. S8 N_2 adsorption-desorption isotherms of conventional SnO_2/CCG composite (square; BET SSA: 177 m^2 g^{-1}), SnO_2/CCG composite derived from the macronanogels (up triangle; BET SSA: 331 m^2 g^{-1}) and dispersed SnO_2/CCG composite derived from the micronanogels (circle; BET SSA: 364 m^2 g^{-1}).

In the MB adsorption technique, 5 ml suspensions of materials were added to 40 ml MB solutions (2.68 x 10^{-5} M). The mixtures were kept in dark for one hour. The liquid was extracted by centrifuge to measure light absorption at $\lambda = 665$ nm. Surface area of the materials was calculated from the deviation of dye concentrations according to the assumption that a single MB molecule covers 1.3 nm^2 surface.[2] The obtained results reveal effective surface areas of 1677 m^2 g^{-1} for micronanogels and 263 m^2 g^{-1} for the calcinated drypowder.

6. Dye adsorption and photodegradation

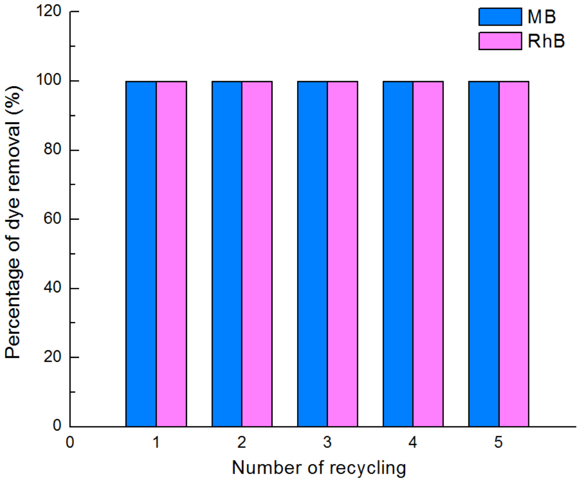

Fig. S9 The recyclability of adsorption and desorption of MB and RhB conducted by the SnO_2/CCG hybrid micro-hydrogels (dye concentration of 10 mg L^{-1}).

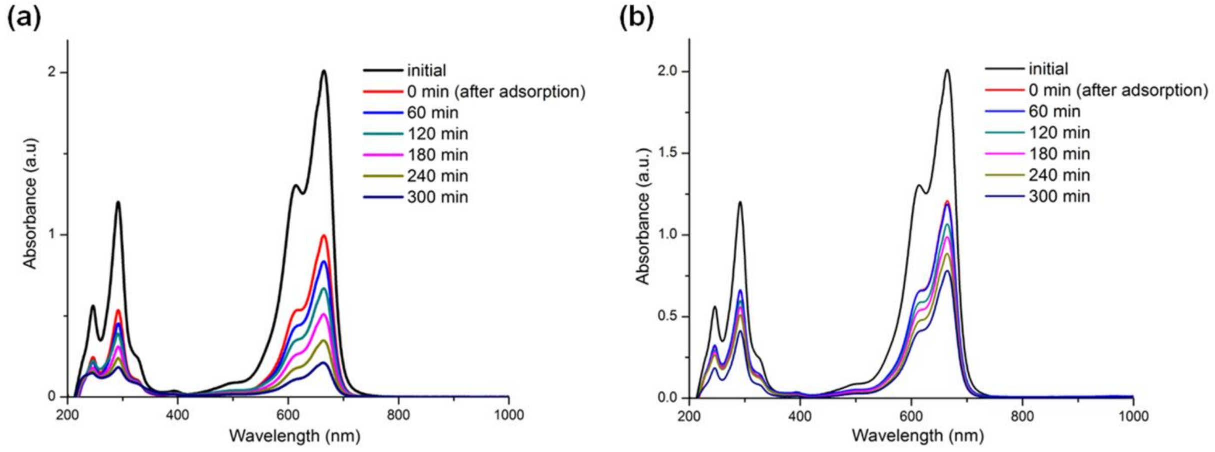

Fig. S10 (a) Absorption spectra of MB adsorption and photodegradation with the presence of micronanogels. (b) Absorption spectra of MB adsorption and photodegradation with the presence of drypowder.

Table S1. Photocatalytic activity of catalysts in MB degradation under visible light

Catalysts	Photodegradation activity (mg mg^{-1} min^{-1} x 10^{-3})	References
N−$K_2Ti_4O_9$−TiO_2	0.029	3
PANI–g-C_3N_4	0.045	4
Fe_3O_4/SiO_2/AuNPs/TiO_2	0.048	5
Graphene/TiO_2	0.078	6
P25-GR	0.144	7
P25-CNT	0.711	8
P25-GR	0.622	8
Drypowder	0.284	This work
Micronanogel	2.5	This work

Note: The photodegradation activity is defined as the weight of dye degraded (mg) over the weight of catalyst (mg) in a unit of time (min).

7. Optical band gap

The optical band gaps were calculated based on UV-VIS absorption spectroscopy (Fig. S11).[9] The band gap of the micronanogel is 1.8 eV, which is much lower than the value of commercial SnO_2 nanoparticles 3.9 eV.

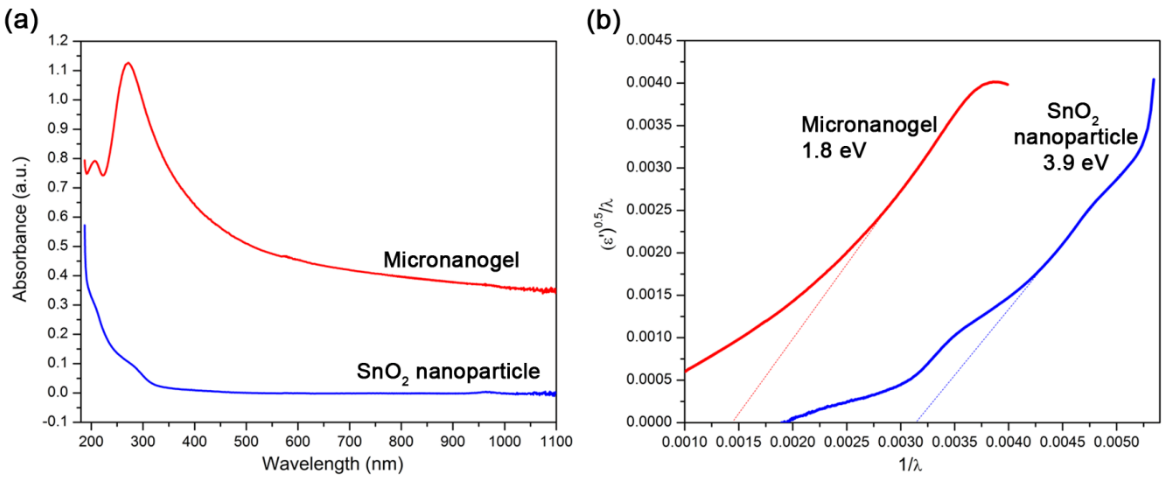

Fig. S11. (a) UV-VIS-NIR absorption spectra of micronanogels and commercial SnO$_2$ nanopaticles. (b) Band gap curves of micronanogels and commercial SnO$_2$ nanoparticles.

From Tauc's equation: $\omega^2\varepsilon' = \left(h\omega - E_g\right)^2$

where ε' is the complex part of the dielectric function which is proportional to the absorbance intensity, $\omega = 2\pi/\lambda$ is the angular frequency of the incident radiation, $E_g = hc/\lambda_g$ is the optical band gap.

The equation can be rewritten as:

$$\frac{\varepsilon'^{0.5}}{\lambda} = \frac{h}{\lambda} - \frac{E_g}{2\pi}$$

The plot of $\varepsilon'^{0.5}/\lambda$ with respect to $1/\lambda$ is linear and intersects the abscissa at the gap wavelength λ_g. The band gap E_g is calculated from the gap wavelength. The plots in Fig. S11b show that the gap wavelengths of commercial SnO$_2$ nanoparticles and micronanogels are 318 and 690 nm respectively. Therefore, the corresponding optical band gaps are 3.9 eV for the SnO$_2$ nanoparticles and 1.8 eV for the micronanogels.

8. Characterization of micronanogel film

SnO$_2$/CCG films were prepared by compressing a layer of micronanogels. The film was dried and then annealed at 200 °C for 1 hour. The obtained micronanogel film was cut into 7x7 mm pieces to characterize the electrical, morphological and elemental properties. Electrical resistance was measured by a 4-point probe instrument in ten times to obtain the balanced value. The average sheet resistance showed the approximate value of 450 mΩ sq^{-1} at room temperature and ambient pressure. The film thickness determined by SEM analysis was 56 μm. The electrical conductivity was calculated using the following equation:

$$\sigma = \frac{1}{\rho} = \frac{1}{R \times A}$$

Where σ is electrical conductivity (S m^{-1}), P is electrical resistivity, R is electrical sheet resistance (Ω sq^{-1}), l is length of the piece of material (m), and A is cross-sectional area of the piece (m^2).

The electrical conductivity of the micronanogel film is 350 ± 10 S cm^{-1}, which is higher than CCG-based thin films 120 ± 10 S cm-1 (Table 1). The SnO_2/CCG platelets in the film were arranged in a compacted 3D structure which is proposed to originate from micronanogel porous scaffolds (Figure S11b).

Table S2. Electrical property of graphene-based materials

Materials	Electrical conductivity (S cm^{-1})	References
Graphene film	100	9
CCG film	160	10
CCG fiber	250	11
CCG fibers	210 – 320	12
CCG papers	118 – 351	13
CCG film	120 ± 10	This work
Micronanogel film	350 ± 10	This work

The relation between electron mobility and electrical conductivity can be described as follow:

$$\sigma = ne\mu_e$$

Where σ is electrical conductivity, n is the number density of electrons, μ_e is the electron mobility.

The electrical conductivity of CCG nanoplatelets is usually low due to lattice defects and insufficient chemical reduction. The formation of SnO_2 nanoparticles on the GO surface, results in the restoration of the π-conjugated network. This restoration as well as the thermal annealing improves the electron mobility in the CCG film. The high electron mobility of the SnO_2 coating (bulk mobility 250 cm^2 V^{-1} s^{-1})[14] might contribute to the enhanced electrical conductivity of the hybrid film.

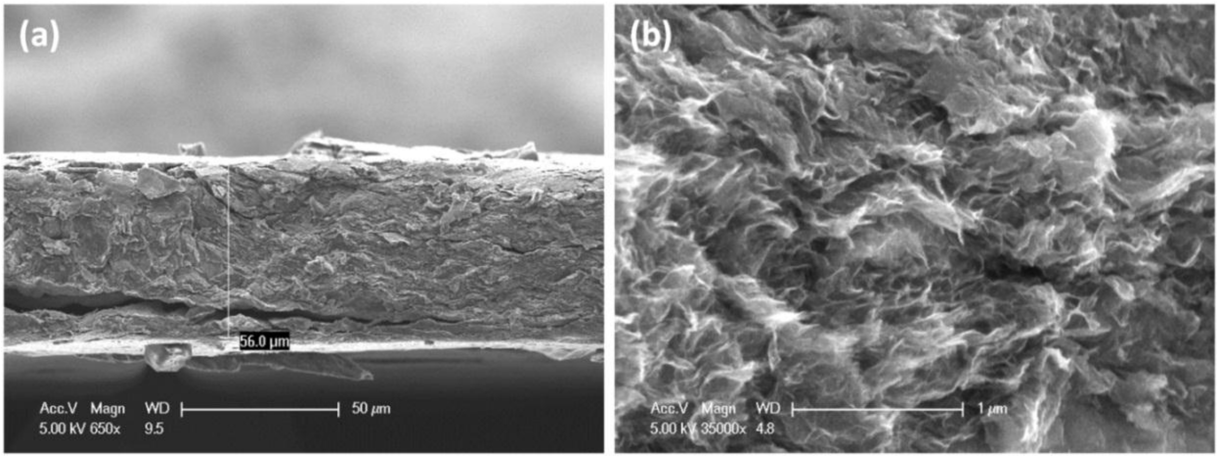

Fig. S12 Cross-sectional SEM images of the micronanogel film: (a) cross-section view and (b) plane view.

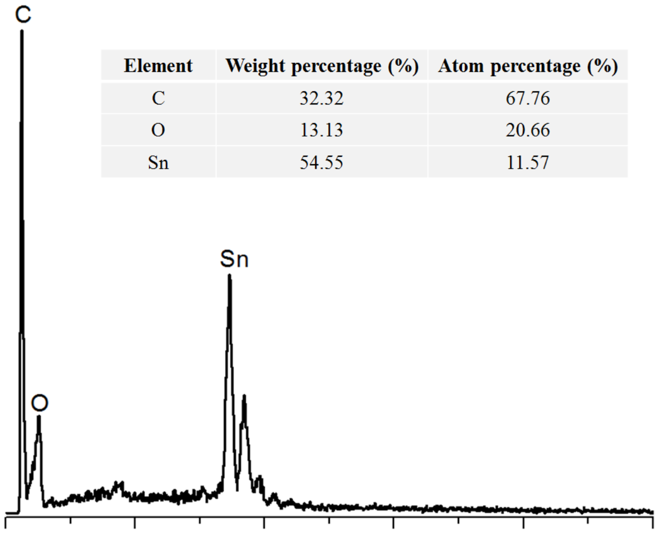

Element	Weight percentage (%)	Atom percentage (%)
C	32.32	67.76
O	13.13	20.66
Sn	54.55	11.57

Fig. S13 EDS for elemental analysis of the micronanogel film.

References:

1 D. Li, M. B. Muller, S. Gilje, R. B. Kaner, G. G. Wallace, *Nat. Nanotechnol.*, 2008, **3**, 101.

2 M. J. McAllister, J.-L. Li, D. H. Adamson, H. C. Schniepp, A. A. Abdala, J. Liu, M. Herrera-Alonso, D. L. Milius, R. Car, R. K. Prud'homme, I. A. Aksay, *Chem. Mater.*, 2007, **19**, 4396.

3 Z. Xiong, X. S. Zhao, *J. Am. Chem. Soc.*, 2012, **134**, 5754.

4 L. Ge, C. Han, J. Liu, *J. Mater. Chem.*, 2012, **22**, 11843.

5 J. Shen, Y. Zhu, X. Yang, C. Li, *J. Mater. Chem.*, 2012, **22**, 13341.

6 D. Zhao, G. Sheng, C. Chen, X. Wang, *Applied Catalysis B: Environmental*, 2012, **111– 112**, 303.

7 H. Zhang, X. Lv, Y. Li, Y. Wang, J. Li, *ACS Nano*, 2010, **4**, 380.

8 Y. Zhang, Z.-R. Tang, X. Fu, Y.-J. Xu, *ACS Nano*, 2010, **4**, 7303.

9 V. Chabot, B. Kim, B. Sloper, C. Tzoganakis, A. Yu, *Sci. Rep.*, 2012, **3:1378**, 1.

10 S. Park, J. An, I. Jung, R. D. Piner, S. J. An, X. Li, A. Velamakanni, R. S. Ruoff, *Nano Lett.*, 2009, **9**, 1593.

11 Z. Xu, C. Gao, *Nat. Com.*, 2011, **2:571**, 1.

12 L. Chen, Y. He, S. Chai, H. Qiang, F. Chen, Q. Fu, *Nanoscale*, 2013, **5**, 5809.

13 H. Chen, M. B. Muller, K. J. Gilmore, G. G. Wallace, D. Li, *Adv. Mater.*, 2008, **20**, 3557.

14 P. Tiwana, P. Docampo, M. B. Johnston, H. J. Snaith, L. M. Herz, *ACS Nano*, 2011, **4**, 5158.